Article:
Bourkoula, A, Constantoudis, V, Kontziampasis, D orcid.org/0000-0002-6787-8892 et al. (4 more authors) (2016) Roughness threshold for cell attachment and proliferation on plasma micro-nanotextured polymeric surfaces: The case of primary human skin fibroblasts and mouse immortalized 3T3 fibroblasts. Journal of Physics D: Applied Physics, 49 (30). 304002. ISSN 0022-3727

https://doi.org/10.1088/0022-3727/49/30/304002

Roughness threshold for cell attachment and proliferation on plasma micro-nanotextured polymeric surfaces: the case of primary human skin fibroblasts and mouse immortalized 3T3 fibroblasts

A. Bourkoula[1]*, V. Constantoudis[2]*, D. Kontziampasis[2]*[+], P.S. Petrou[1], S.E. Kakabakos[1], A. Tserepi[2], E. Gogolides[2]

[1]Immunoassay/Immunosensors Lab, Institute of Nuclear and Radiological Sciences and Technology, Energy and Safety, NCSR "Demokritos", 153 41 Aghia Paraskevi, Attiki, Greece

[2]Institute of Nanoscience & Nanotechnology, NCSR "Demokritos", 153 41 Aghia Paraskevi, Attiki, Greece

*These authors contributed equally in this study.

[+]Author current address: Institute of Particle Science and Engineering (IPSE)
School of Chemical and Process Engineering (SCAPE)
Room 2.15, Engineering Building,
University of Leeds,
Leeds, LS2 9JT, UK

Corresponding author: Dr Evangelos Gogolides
Institute of Nanoscience and Nanotechnology
NCSR "Demokritos"
Patriarhou Gregoriou & Neapoleos 27 Street
Aghia Paraskevi, Attiki, Greece 153 41
Tel: +30-210-6503237, fax: +30-210-6511723
E-mail: e.gogolides@inn.demokritos.gr

Abstract

Poly(methyl methacrylate) surfaces have been micro-nanotextured in oxygen plasmas with increasing ion energy, leading to micro-nanotopography characterized by increased root mean square roughness, correlation length and fractal dimension. Primary Human skin fibroblasts and mouse immortalized 3T3 fibroblasts were cultured on these surfaces and the number of adhering cells, their proliferation rate and morphology (cytoplasm and nucleus area) were evaluated as a function of roughness height, correlation length, and fractal dimension. A roughness threshold behavior was observed for both types of cells leading to dramatic cell number decrease above a threshold, which is almost similar for the two types of cells, despite their differences in size and stiffness. Results are discussed based on two theoretical models, which are reconciled and unified when the elastic moduli and the size of the cells are taken into account.

1. Introduction

In vivo, cells are never exposed to flat surfaces, but reside in an environment composed of wide ranges of nanoscale surface roughness and submicrometer sized fibrils, since the basement membranes of tissues exhibit nanotopographies which interact with cells [1]. It is therefore very important to be able to create nanostructured surfaces that are more biomimetic compared to standard flat culture surfaces [2]. The recent developments of micro- and nano-fabrication technologies offer many possibilities for the application of nanostructured surfaces in the fields of tissue engineering [3, 4], medical prosthetics [5], biochips for diagnostics [6, 7], and cell microarrays [8].

Many techniques have been developed for the fabrication of substrates with controlled nanoscale topography and surface chemistry [9], such as electron beam lithography [10], colloidal lithography [11], dip-pen lithography [12], micro-contact printing [13], polymer demixing [14], photolithography [5] and electrospinning [15]. However, the requirement for rapid and reproducible fabrication of nano-features at low cost is met only by a few methods. Plasma treatment is such a method, due to the number of parameters that can be altered to achieve the desired morphological and chemical effects. Changing feed gas in the plasma, and bias voltage (which determines the energy of the positive ions inducing ion-enhanced etching of the substrate) one may have different modification ranging from deposition to etching, nanotexturing, chemical modification, and consequently wetting control [16-20]. Plasma etching and plasma nanoassembly enables fast (within a few minutes) fabrication of random or quasi-ordered nanostructures on polymeric surfaces [21-23].

There are numerous experimental studies on the effect of surface topography (both random and ordered) on cell behavior leading to a variety of conclusions mainly due to the high number of parameters that could affect cell behavior (cell type, feature size and geometry, properties of the bulk material, etc.) [1, 5]. In particular, some works report an increase of cell adhesion and proliferation with roughness [24], while others indicate the existence of an optimum range of roughness to efficiently capture cells and enhance their adhesion and proliferation [25, 26]. On the other hand, there are reports that show the opposite behavior with reduced cell growth on largely rough substrates [27-32]. Besides the impact of roughness, induced mechanical stimuli on cell adhesion and proliferation, it is important to know the effects on the inner cell structure since these changes may control the adhesion process. However, while there are several reports discussing cell adhesion and proliferation on rough surfaces, there are only a few reports discussing the effects of roughness on the morphology of the cytoplasm and the nucleus [33, 34].

The above mentioned variety of results and conclusions makes it difficult to summarize the effect of nanotopography on cell behavior in a concise and complete framework. Despite this difficulty, in a recent study Decuzzi and Fereira [35] elaborated a theoretical model to improve our understanding on cell – topography interaction and offer a unified explanation of the above diverse results. Their approach is mainly based on the estimation of the free energy balances between cell membrane and substrate surface, assuming that cells are thin elastic layers with specific Young modulus (E), which reside on a solid rough surface with periodic morphology. In particular, a critical roughness threshold exists above which cells cannot survive on the topography. The threshold is shown to be inversely proportional to E, which means that given similar adhesion forces, less rigid cells (with smaller E) adhere more on the substrate protrusions and have a higher threshold.

A different model has been motivated by the bactericidal property of the nanopatterned Cicada wing surfaces and developed by E.P. Ivanova and her group [36, 37]. They proposed that the adsorption of the bacterial cells on the nanopattern of cicada wing may lead to a drastic enhancement of their area causing the stretching of cell membrane. When the stretching exceeds some threshold, it can cause the irreversible rupture of cell surface and its death. According to this modeling approach, the less rigid (i.e. with small E) bacterial membranes are more sensitive to the bactericidal mechanism of the wings and present increased death rates.

The impact of cell membrane stiffness on cell adhesion differentiates the two models since they predict opposite trends. A combination of the effects of both models (increased adhesion and stretching) can lead to milder dependencies of critical roughness threshold on cell stiffness. An experimental verification of the synergetic role of both effects would require to culture cells with different stiffness and similar adhesion forces on the same series of surfaces with increased roughness. This is what this work is aiming towards.

In particular, the goal of this work is to evaluate the effect of surface roughness on the attachment and proliferation of two different types of fibroblasts, namely human primary skin fibroblasts and mouse 3T3 immortalized fibroblasts, and discuss the results with respect to the free-energy based theoretical scheme. The selection of the specific cells was based on the fact that although they are both fibroblasts and could be cultured under common conditions they differ considerably in size and stiffness, with the human skin fibroblasts to be considerably bigger and more elastic than the mouse immortalized fibroblasts [38]. In addition to cell adhesion and proliferation, here the surface roughness effects on the morphology of both the cytoplasm and the nucleus of cells are also determined, so as to inspect in more details the

very nature of cell response caused by roughness undulations. The rough substrates we employed in this study were poly(methyl methacrylate) (PMMA) films treated and micro- and nano-textured by oxygen plasma with a root mean square surface roughness R_{rms} from ~5 to 40 nm depending on the treatment time. A threshold behavior is demonstrated regarding cell adhesion, proliferation as well as cell morphological characteristics versus topography, and these findings are reconciled with the theoretical calculations mentioned above. Although PMMA is not a commonly used biomaterial for cell cultures, it is extensively used for microfluidics and lab-on-a-chip fabrication. It is therefore very important for those working with cells on chip to know the PMMA cell binding properties, given the great interest for incorporation of such "smart" surfaces into microfluidics [20].

2. Methods

2.1 PMMA surface preparation

Poly(methyl methacrylate) (PMMA) with molecular weight of 120 kDa (Sigma-Aldrich Co; Taufkirchen, Germany) was dissolved at 30% (w/w) in anhydrous Propylene Glycol Methyl Ether Acetate (PGMEA) and spin-coated on Si wafers (1000 rpm for 30 s with acceleration of 300 rpm/s^2), resulting in a film thickness of ~20 μm. After spin-coating the wafers were baked at 90 ^{o}C for 20 min and then at 150 ^{o}C for 1h. Etching was performed in a high density helicon plasma reactor (MET system from Alcatel-Adixen) at the following conditions: Oxygen gas flow rate 100 sccm; operating pressure 0.75 Pa; electrode temperature 60 ^{o}C; bias voltage varying from -25 to -100 V (to find the value of ion energy the plasma potential of 15-25 V should be added to the absolute value of the bias voltage, e.g., 25V+15V, or 100V+15V). The etching time was in all cases 1 min and the etching rate varied between 500-1500 nm/min depending on the bias voltage. Temperature was controlled by helium backside cooling of a carrier wafer on which samples were glued with thermal paste.

2.2 Surface characterization

PMMA surfaces were analyzed by a CP-II AFM instrument from Veeco (Plainview, NY). All AFM measurements were performed in (non-contact) tapping mode using PPP-NCHR-50 tips with radius of curvature less than 10 nm. The obtained surface measurements have the form of measured heights on a x-y square lattice $z(x_i,y_j)$ where $i,j=1,\ldots,N$. In our measurements $N = 512$ while the scanning range (lattice area) has been 2x2 μm^2. Due to the random and complex nature of surface morphologies statistical analysis, as well as mathematical

transformations are needed for their characterization. To this end, the software nanoTOPO-AFM was used (Nanometrisis; Athens, Greece, www.nanometrisis.com), which delivers several roughness metrics characterizing both vertical (amplitude) and spatial (frequency) aspects of surface morphology. In this work, the focus was on three parameters, root mean square (rms), correlation length and fractal dimension, which define the most dominant features of surfaces. Rms value quantifies the amplitude of height fluctuations on surfaces and with the mean amplitude R_a they constitute the most common roughness parameters. In a more mathematical perspective, rms is the second order moment of the surface height distribution function. The second parameter is the correlation length ξ which defines the lateral distance beyond which the in-plane surface height correlations degrade to noise levels. In surfaces with random distribution of well-defined mounds, the correlation length can be used as an estimator of the average mound width. The fractal dimension d_f can be calculated in fractal surfaces exhibiting self-similar (more precisely self-affine) symmetry and quantifies the relative contribution of high frequency fluctuations to the total surface roughness. The triplet of these parameters (rms, ξ, d_f) constitute the so-called three-parameter model which has been extensively used in the characterization of sidewall roughness in nanoelectronic structures [39].

In order to probe the chemical modification of the surface by the plasma, Fourier Transform Infrared Spectroscopy (FTIR) was performed with a Thermo Scientific Nicolet 6700 FT-IR instrument using attenuated total reflection (ATR) technique (128 scans, resolution of 4.0 cm^{-1}, data recorded from 4000 cm^{-1} to 450 cm^{-1}).

2.3 Cell culture

Primary human skin fibroblasts and Swiss albino mouse immortalized 3T3 fibroblasts were obtained by the American Type Culture Collection. Cells were grown in Dulbecco modified Eagle medium (DMEM) supplemented with 10% (v/v) heat-inactivated fetal bovine serum (FBS), 2 mM L-glutamine, and 1% (v/v) penicillin/streptomycin solution at 37 ^oC in a saturated humid atmosphere containing 95% air and 5% CO_2. When cells reached 70-80 % confluence, they were detached from the culture flasks through treatment with 0.25 % (w/v) trypsin/EDTA solution and re-suspended in DMEM.

2.4 Cell adhesion experiments

Untreated and plasma nanotextured PMMA surfaces were used as substrates to culture mouse immortalized 3T3 fibroblasts and primary human skin fibroblasts. The plasma treated PMMA

surfaces were left to age for at least 10 days prior to use so as to reach a constant contact angle very close to that of untreated PMMA (~67º). The wafers with the PMMA films were cut to 1x1 cm^2 pieces. These pieces were sterilized prior to cell seeding by exposure to ultraviolet light for 20 min and placed in 24-well culture plates. For seeding 1 mL of cells suspension at a density of 25,000 cells/mL was added in each well. The culture medium in the wells was renewed every 24 h. To determine the number of attached cells, the substrates were washed with 10 mM phosphate buffer saline, pH 7.4 (PBS), in order to remove the non-adhered dead cells. Then, the cells were fixed with 4% (w/v) paraformaldehyde solution in PBS for 20 min at room temperature (RT). The fixed cells were rinsed 3 times with PBS and incubated with a 50 ng/ml of 4',6-diamidino-2-phenylindole (DAPI; Sigma-Aldrich Co., Taufkirchen, Germany) in PBS for 10 min at RT to stain the cell nucleus. Thereafter, coverslips were mounted on top of the substrates using p-Phenylenediamine antifade mounting gel (Vectashield; Vector Laboratories Inc., Burlingame, CA). The substrates were observed using an epifluorescence microscope (Axioskop 2 Plus; Carl Zeiss, Hamburg, Germany) facilitated with a filter pair with appropriate excitation/emission maximums for DAPI (365/420 nm) and a CCD camera (MicroPublisher 3.3 RTV; QImaging, Surrey, BC, Canada) for image acquisition. For each surface 25 images were obtained, each one covering a 1725x1291 μm^2 area. From these images the stained cell nuclei were counted using Image ProPlus v6.0 software (Media Cybernetics, Inc.; Rockville, MD). Experiments were performed three times in quadruplicate and the numbers of cells counted were averaged and expressed as cells/cm^2 (mean ± standard deviation). The results were analyzed statistically by paired Student's t-test method and considered significantly different at p values lower than 0.05.

2.5 Cell morphological analysis

Fluorescence staining was employed to image the cytoskeleton and the nucleus of the primary human skin and mouse immortalized 3T3 fibroblasts adhered on the different PMMA surfaces after 3 days of culture. For this purpose after washing and fixing of cells with paraformaldehyde as described in 2.4, the cells were rinsed 3 times with PBS and permeabilized through incubation with 0.1% (v/v) Triton X-100 in PBS for 10 min. After gentle washing with PBS, the cells were blocked with 5% (v/v) bovine serum albumin solution in PBS for 1h at RT, and then washed with PBS. To visualize the cytoskeleton, F-actin was stained through reaction with a 150 nM Phalloidin Atto 488 (Sigma-Aldrich Co.; Taufkirchen, Germany) solution in PBS for 1 h, followed by washing with PBS. Staining of the nucleus with DAPI and mounting of the coverslips was performed as described in 2.4.

Fluorescence images were obtained using two filter pairs with appropriate excitation/emission maximums (365/420 nm for DAPI, 493/520 nm for Atto 488). Images covering a 430 x 325 μm^2 area were obtained, and the cytoplasm and nucleus area of at least 200 random individual cells per substrate were calculated using the Image ProPlus v6.0 software. Experiments were performed three times in quadruplicate, and the cells cytoplasm and nucleus area determined were averaged and expressed as mean value ± standard deviation.

3. Results

3.1 Oxygen plasma micro-nanotextured surfaces with increasing roughness

PMMA substrates were etched in oxygen plasma for 1 min using four different bias voltages (-25, -50, -75 and -100 Volts) while keeping all other parameters fixed. The plasma treatment causes gradual roughening of the etched PMMA surfaces, while roughness parameters (rms, ξ, d_f) grow with bias voltage as shown in Figure 1a. All roughness parameters exhibit a correlated behavior with an almost linear growth versus bias voltage. This means that at high bias voltages the roughness (texture) becomes higher, with wider features, and with higher frequency undulations on these features. Detailed AFM imaging was presented in one of our previous publications [34].

The plasma modifies both the surface topography and the surface chemistry. Detailed XPS analysis of oxygen plasma treated PMMA has been discussed in detail in our previous work [17, 41]. Here, in Fig. 1b we also present FTIR data to show the plasma modification. The FTIR spectra of PMMA confirmed the presence of various bonds in the structure (see Figure 1b). PMMA give a series of characteristic infrared bands at 2950, 1722, 1435, 1386, 1238, 1190, 1142, 986, 840, 810 and 751 cm^{-1} [42,43]. Although the two spectra revealed similar peaks, there are differences in the peak height as shown in the Fig. 1b. The bands at 2950 and 1145 cm^{-1} assigned to CH stretching, and CH_2 bending, respectively, are reduced in size (transmittance increases) due to etching of the material and oxidation of the surface. On the contrary the intense band at 1721 cm^{-1} assigned to C=O stretching (skeletal mode), and the medium size band at 750 cm^{-1} assigned to the C=O in plane and out of plane bending, increase in size (transmittance decreases) due to the strong surface oxidation to CO and COOH groups.

a

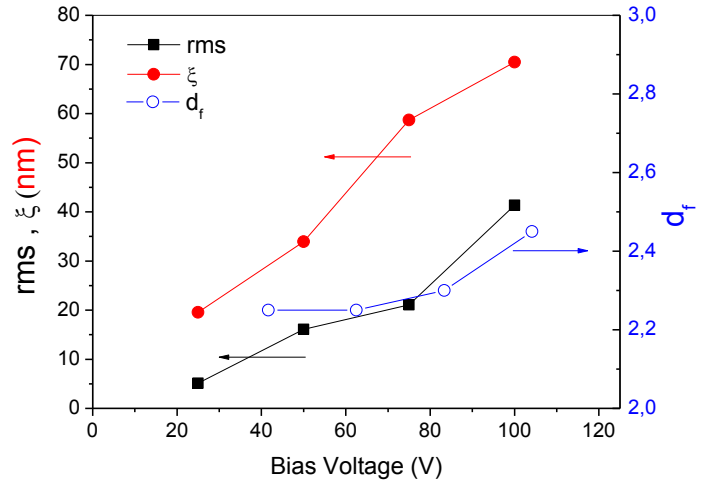

b

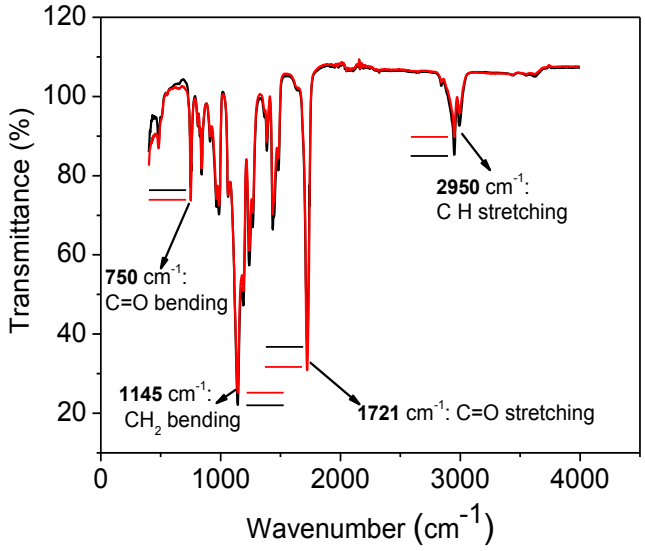

258 **Figure 1**. a) Surface roughness parameters of PMMA surfaces micro-nanotextured in Oxygen
259 plasma (rms, correlation length ξ, and fractal dimension d_f) versus bias voltage. Notice the
260 correlated behaviour of all roughness parameters which show an almost linear increase with
261 bias voltage. b) ATFTIR spectra of untreated (black line) and plasma treated PMMA films
262 (red line). Notice the reduction of the CH and CH_2 peaks and the increase of the C=O peaks
263 after plasma treatment.

264

265

266

3.2 Adhesion and proliferation of primary human skin and mouse immortalized 3T3 fibroblasts on oxygen plasma micro-nanotextured PMMA surfaces

The micro-nanotextured PMMA surfaces along with the untreated ones were used as culture substrates for primary human skin fibroblasts or mouse immortalized 3T3 fibroblasts. After one and three days of culture under standard conditions, the number of cells on the different surfaces was determined. Concerning skin fibroblasts after 1 day of culture, it was found that similar numbers of cells were adhered on all plasma treated and untreated surfaces (5890±524 cells per cm^2). After 3 days of culture, as shown in Figure 2(a-c), the number of skin fibroblasts on the untreated as well as on substrates with rms, ξ and d_f values lower than or equal to 21.1 nm, 40 nm and 2.25, respectively, was increased by a factor of approximately 2. On the contrary, when they were cultured on the more roughened substrates (rms=41.4 nm, ξ=70.4 nm and d_f=2.45 nm) a significant reduction of the number of attached cells was observed compared to surfaces with lower roughness. In detail, the number of attached cells per unit area was almost half in the strongly rough substrates with respect to the surfaces with lower or no roughness at all (untreated PMMA films).

The picture changes slightly when we move to 3T3 cells. After 1 day of culture, the number of cells adhered on plasma treated surfaces were similar and at least 4-times higher (6938±789) than the number on the untreated PMMA surface (1664±312). Nevertheless, looking at the cell densities after three days of culture (red squares in Figure 2), we noticed that similarly to fibroblasts, the strongly rough substrates (rms=41.4 nm, ξ=70.4 nm and d_f=2.45 nm) are hostile for 3T3 and the density drops to almost 60% of the surfaces with smaller roughness. In contrast, the number of cells on the untreated PMMA after 3-days of culture is almost 2-times higher than that determined for 1-day of culture. Thus, in order to deduce differences in cell behavior due to plasma treatment, the proliferation rate was determined as the ratio of the number of cells counted on a particular surface after 3 days of culture to the number determined after 1 day of culture.

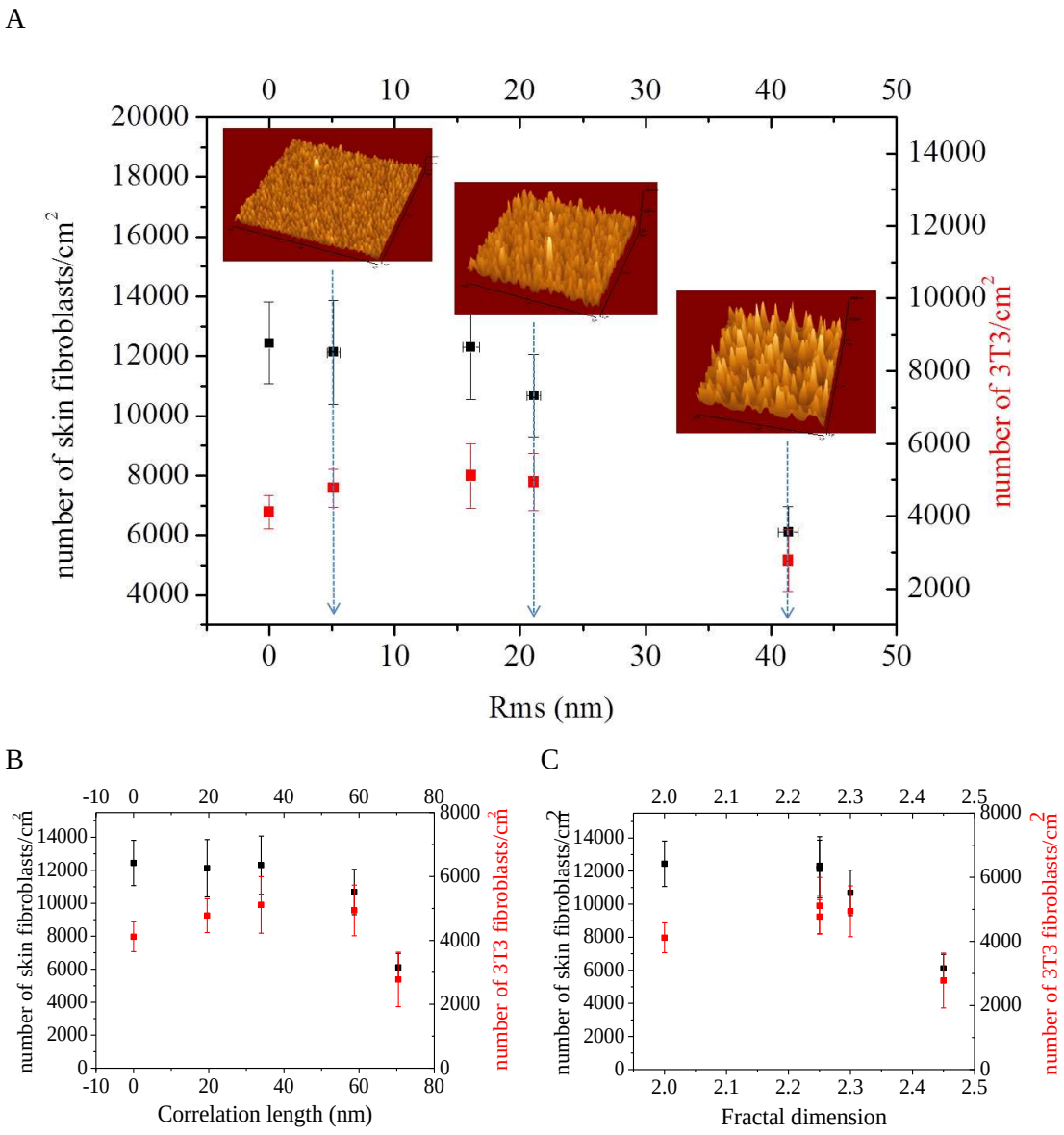

Figure 2. The number of primary skin fibroblasts (black full squares) and 3T3 cells (red full squares) per surface unit as a function of surface rms (a), fractal dimension (b), and correlation length (c) after 3 days of culture. AFM images of surface topography are shown in Figure 2(a) for 3 substrates with 3 different rms values (left 5.14 nm; center 21.1 nm; and right 41.4 nm). Each point is the mean value of three independent experiments performed in quadruplicate ± SD.

The proliferation rate versus the rms value of the different PMMA substrates (shown in Figure 3) demonstrate that for the primary skin fibroblasts the rate was decreased approximately by 50% when cells were cultured on the PMMA surface with the highest nanostructure (rms=41.4 nm) compared to all the other nanotextured (rms=5.14-21.1 nm) as

well as the untreated PMMA surfaces which exhibited proliferation rates of about 2 (see black squares in Figure 3). On the other hand, the proliferation rates determined for 3T3 demonstrate that even a slight roughening of PMMA substrates (rms=5.14 nm) influences negatively the proliferation of cells since the rate was three-fold lower on the surface with the lowest roughness (proliferation rate=0.7) compared to the one determined for the untreated PMMA surface (proliferation rate=1.9, not shown in Figure 3). Similar proliferation rates were obtained for surfaces with rms, ξ and d_f values lower than or equal to 21.1 nm, 40 nm and 2.25, respectively, whereas for the surface with the higher roughness (rms=41.4 nm, ξ=70.4 nm and d_f=2.45 nm), the rate was dropped to less than 0.5. Rate values smaller than 1 suggest that the roughening of PMMA substrates promotes cell death, and therefore leads to a net reduction of their population. Thus, concerning the rough substrates, an rms value higher than 21.1 nm, seems to affect negatively the proliferation of both skin fibroblasts and 3T3 cells. The fact that for 3T3 cells the proliferation rates for all plasma treated surfaces are lower than that on the untreated ones could be ascribed to a different response to surface chemistry of plasma treated PMMA. The above results for both cell adhesion and proliferation rate reveal the existence of a threshold in roughness parameters above which the surface roughness has detrimental effect on cell capture and proliferation.

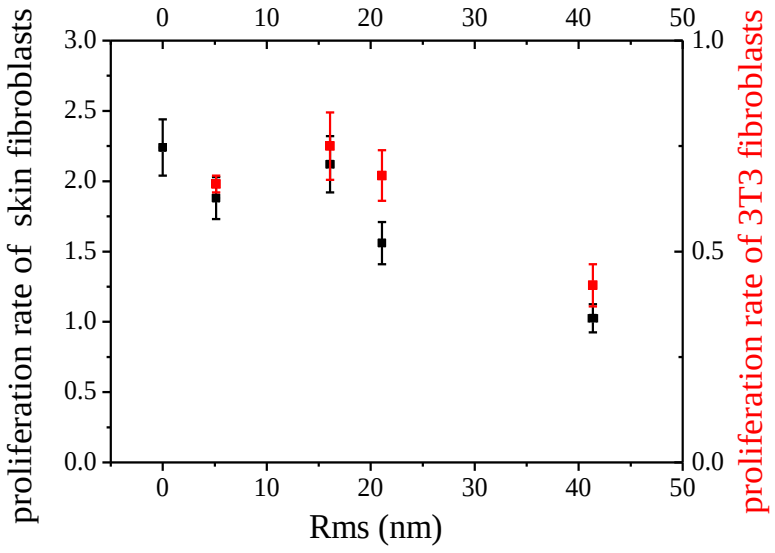

Figure 3. Cell growth assessment of primary skin fibroblasts (black squares) and immortalized 3T3 fibroblasts (red squares) after culture on untreated PMMA (rms=0 nm) and on different nanotextured PMMA surfaces of increasing roughness. The proliferation rate of 3T3 cells on untreated PMMA surface (1.9±0.1) is not shown in the plot in order to visualize more clearly the cells behavior on the rough surfaces. Each point is the mean value of three independent experiments performed in quadruplicate ± SD.

3.3 Effect of PMMA surface roughness on primary human skin and mouse immortalized 3T3 fibroblasts morphology

Further to cell attachment and proliferation, the effect of surface micro-nanotexturing on cell and nucleus size was evaluated. For this purpose, double fluorescence staining of cytoskeleton F-actin and cell nucleus was employed. Concerning skin fibroblasts, it was found that the cell cytoplasm area (Figure 4(a)) and morphology remained unaffected when the cells grew for 3 days on untreated PMMA, as well as on nanotextured PMMA surfaces with rms values lower than or equal to 21.1 nm (Figure 4(b1) & 4(b2)). On the contrary, when the cells were grown on the nanotextured PMMA surface with rms of 41.4 nm a significant distortion of their cytoplasm was observed (Figure 4(b3)). It is worth noticing that on the roughest PMMA surface, the cells cytoplasm area was reduced approximately 2.5 times compared to the cytoplasm area determined for cells grown on either untreated or plasma treated PMMA surfaces of lower roughness (Figure 4(a)). This is evident from the representative cell images grown on nanotextured PMMA surfaces with rms values 5.14 nm, 21.1 nm and 41.4 nm, provided in Figures 4(b1), 4(b2), and 4(b3), respectively. From the images it is also evident that when the cells have been grown on surfaces with rms values lower than or equal to 21.1 nm, they were well spread on the surface and extend many filopodia-type extensions. In addition, the F-actin filaments were well organized and oriented along the cell long axis. On the other hand, the cells that have been cultured on the roughest surface (rms value 41.4 nm) were significantly shrunk with no apparent F-actin organization and only few and short filopodia-type extensions can be observed. Similarly to cell cytoplasm, the nucleus was significantly shrunk (~40%) compared to other surfaces only when the cells were cultured on the roughest surface (Figure 4(a)).

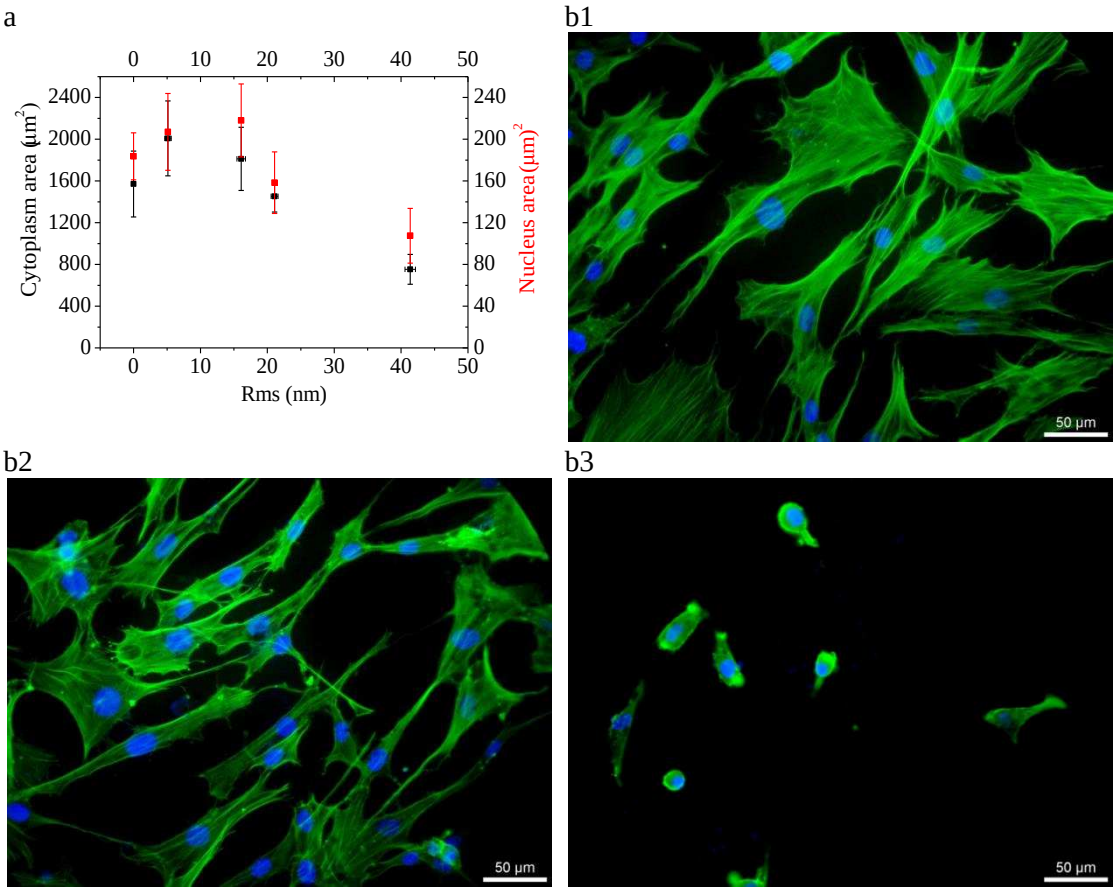

Figure 4. a) Cytoplasm and nucleus area of primary skin fibroblasts cultured for three days on PMMA surfaces versus surface roughness (Rms). Each point is the mean value of three independent experiments performed in quadruplicate ± SD. b) Fluorescence microscope images of primary skin fibroblasts (nuclei: blue; cytoplasm: green) cultured for three days on oxygen-plasma nanotextured PMMA surfaces with rms 5.14 nm (b1), 21.1 nm (b2) and 41.4 nm (b3).

Regarding 3T3 immortalized mouse fibroblasts, distinct differences in cell morphology were evident between cells cultured for 3 days on untreated and nanotextured surfaces with rms values ranging up to 16.1 nm compared to those cultured on surfaces with higher roughness (21.1 to 41.4 nm). As demonstrated in Figure 5(a), the cytoplasm area was reduced when cells were cultured on PMMA surfaces with rms values equal to or higher than 21.1 nm, compared to those cultured on surfaces with lower roughness or untreated PMMA surfaces. In particular as shown in Figure 5(a), the mean cytoplasm area of cells cultured on surfaces with rms value of 21.1 nm was reduced by 30% compared to that of cells cultured on untreated or PMMA surfaces with rms values of 5.14 and 16.1 nm, and by 60% when cells were cultured on the

roughest surface (rms 41.4 nm). Representative fluorescence images of 3T3 cells cultured for 3 days on nanotextured PMMA surfaces with rms values of 5.14 nm, 21.1 nm and 41.4 nm, are provided in Figures 5(b1), 5(b2) and 5(b3), respectively. The cells presented normal morphology with well spread cytoskeleton on untreated PMMA surface as well as on substrates with rms values ranging between 5.14 and 16.1 nm. The cytoskeleton of 3T3 cells begun to shrunk when they were cultured on PMMA surfaces with rms ≥21.1 nm (Figure 5(b2)) and they presented the maximum shrinkage on the roughest PMMA (Figure 5(b3)). Nevertheless, opposite to the human skin fibroblasts, the shrinkage of the cell cytoplasm was not accompanied by shrinkage of the nucleus in the case mouse immortalized 3T3 fibroblasts.

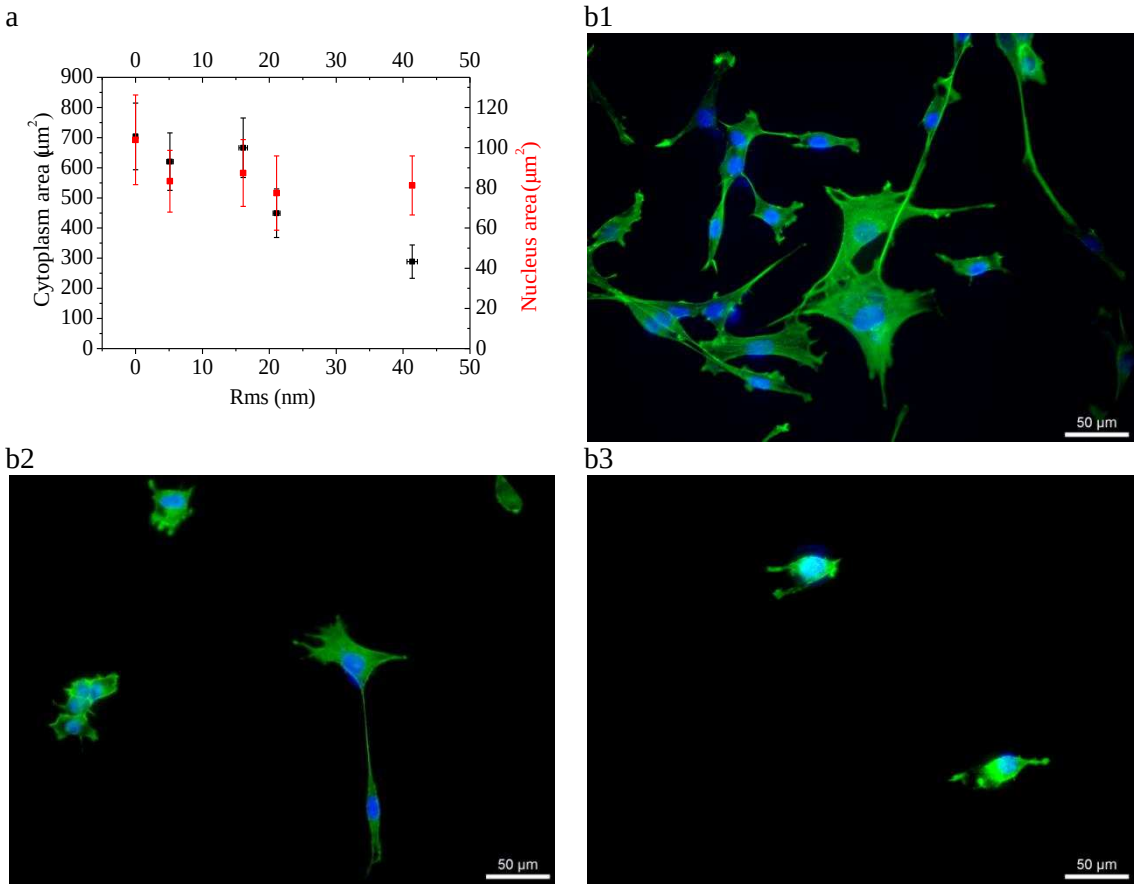

Figure 5. a) Cytoplasm and nucleus area of immortalized 3T3 fibroblasts cultured for three days on PMMA surfaces versus surface roughness (Rms). Each point is the mean value of three independent experiments performed in quadruplicate ± SD. b) Fluorescence microscope images of immortalized 3T3 fibroblasts (nuclei: blue; cytoplasm: green) cultured for three days on oxygen-plasma nanotextured PMMA surfaces with Rms 5.14 nm (b1), 21.1 nm (b2) and 41.4 nm (b3).

4. Discussion

Recently several efforts have been undertaken towards an integrated framework for understanding the impact of substrate morphology on cell adhesion. In the Introduction, we made reference of two prominent theoretical approaches which elaborate a more biophysical view of cell-surface interactions differentiating from the previous more biochemically-oriented argumentations, since they consider them as interactions between an elastic biolayer (cell membrane) and an inert solid rough substrate [35-37]. The basic theoretical prediction of both models is the reduction of adhesion on substrates with large roughness (rms) above a critical threshold value of rms_{cr} roughness. Below this threshold, we can have either insensitivity of cell adhesion to roughness or a broad maximum indicating an optimum surface roughness range for capturing cells. However, the two models and the mechanisms they recall for explanation of experimental findings differ on the role of cell stiffness (Elastic modulus E). According to the model proposed by Decuzzi and Ferrari [35], the rms_{cr} is inversely proportional to adherent cell stiffness (E), which means that cells with less stiff membranes require more substrate roughness to start reducing their adhesion strength. On the other hand, the second model [36, 37] makes the opposite prediction and explains that the bacteria cells with less stiff (smaller E) membranes suffer from more stretching and therefore increased deterioration.

Looking again at the diagrams of Figure 2, one can realize that our experimental measurements fit at least qualitatively with the basic theoretical predictions: both cell series suffer from a reduction of their adhesion strength at the most rough substrates, with a critical threshold roughly defined by rms_{cr}=20 nm, ξ_{cr}=40-50 nm and $d_{f,cr}$=2.3. Below the critical threshold, the adhesion of 3T3 series exhibits a broad maximum, while skin fibroblasts remain almost insensitive to substrate morphology changes. A threshold-like behaviour is also observed in the dependencies of proliferation rate and cell cytoplasma and nucleus area on substrate roughness (see Figs, 3, 4 and 5 respectively) since the PMMA surfaces with high roughness deteriorate cell proliferation and reduce cytoplasma and nucleus spatial structure. Therefore, the threshold in substrate roughness at rms_{cr}=20 nm, ξ_{cr}=40-50 nm and $d_{f,cr}$=2.3 impacts the whole aspects of cell life (adhesion, proliferation) and morphology (cytoplasma and nucleus area). As referred above, this experimental finding agrees with the theoretical predictions discussed in [35-37]. What needs more elucidation is the observed similarity of threshold roughness values in the two cell series given their difference in membrane stiffness.

According to [38] the Young modulus of skin fibroblast cells is on average almost the half of the modulus of 3T3 cells (~ 900 versus 1800 Pa). Given the expected similarity of the strength of specific and nonspecific interactions in both cell types, the difference in cell rigidities should have led to much larger roughness thresholds in skin fibroblasts. What is the extra effect preventing it and causing the reduction of roughness threshold in this cell line?

At this point, we can recall the second modelling approach elaborating to explain the bactericidal nature of cicada wing surface structures. As explained in the Introduction, the adsorption of a bacteria cell on the surface structures of cicada wings could cause a drastic stretching of the cell membrane especially on the suspended part between the contact points, which could lead to irreversible cell membrane rupture and bacteria death. According to this model, the less stiff the cell membrane is, the more detrimental is the effect of roughness and the probability to rupture the cell membrane and cause its death. In addition to the stiffness effect, a theoretical approach based on this model, has also shown that the detrimental stretching of cell membrane is proportional to cell weight and size [40]. Taking into account that the size of skin fibroblasts is almost twice the size of 3T3 cells, there is one more factor causing the stretching effects to be much more severe in the fibroblasts than in the 3T3 cells. A schematic of the membrane shape of both cell types when they are residing on a rough substrate is illustrated in Figure 6. In this figure, it is shown that the smaller stiffness and the larger size of skin fibroblasts favour larger adhesion areas on the summits of rough substrates than the 3T3 cells. However, the same features (less stiffness and larger size) lead to stronger stretching of cell membranes suspended between contact areas, which deteriorate cell behaviour. These two effects can counteract each other providing an explanation of the observed similarity of roughness thresholds in the number of captured cells (adhesion strength) in the two series.

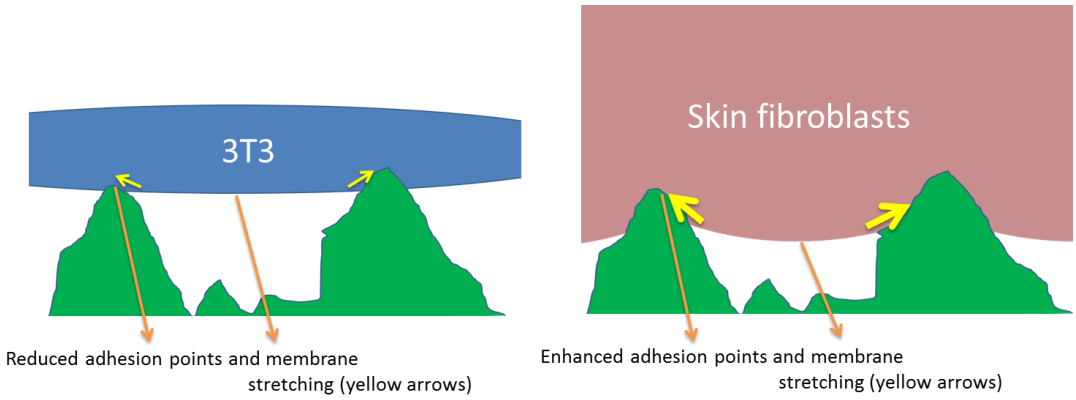

Figure 6. Schematic diagram of the membrane shapes of a 3T3 (left) and a fibroblast (right) cell residing on a rough substrate. Due to the much larger stiffness and smaller size, 3T3 cell

is expected to develop less adhesion area with the substrate and to exhibit less stretching between contact points than the skin fibroblasts (marked by the different width of yellow arrows). The detrimental effect of increased stretching in skin fibroblasts can counteract the enhanced adhesion areas and explain the similarity of roughness thresholds in two cell types.

The large stiffness of 3T3 cells can be also responsible for their reduced proliferation rates on rough substrates with respect to those on flat surfaces (see 3.2). As shown in Figure 6, 3T3 cells are expected to exhibit a contact point configuration with the rough substrate due to their large Young modulus which may lead to decreased adhesion strengths even for low values of roughness.

A final comment concerns the role of substrate fractal dimension on cell adhesion. A recent study has provided evidence that more fractality on substrate morphologies favors cell adhesion [32]. On the contrary, here we observe that the strongly roughened substrates which are characterized by increased fractal dimension are hostile to cell adhesion and give smaller cell densities and proliferation rates. Following the authors of above ref. [32], we should emphasize that the effect of fractal dimension is correlated to those of the height and width of surface fluctuations as quantified by rms and ξ respectively. In our experiments, the surfaces are modified by changing the bias voltages of plasma etching process and this lead to a collective increase of all roughness parameters rms, ξ and d_f. Therefore, the large fractal dimensions go with large rms and ξ values and we cannot see the bare effect of fractal dimension at moderate roughness as suggested in [32]. The concluding message is that in order to get a safe decision for the effects of a specific roughness parameter on cell adhesion, we should be able to create surfaces on which we control the changes of this parameter in an independent way. Otherwise, the effects of less important parameters (such as fractal dimension) can be overwhelmed by the more dominant ones such as rms roughness.

5. Conclusions

Primary human skin fibroblasts and immortalized mouse 3T3 fibroblasts have been cultured on oxygen plasma treated PMMA surfaces with random or quasi-ordered structures of increasing roughness. The effect of surface roughness on the number of adhered cells, their proliferation rate, as well as the morphology of cell cytoplasm and nucleus was determined. Although the two cell types behaved differently on the rough surfaces, a common roughness threshold was determined for surfaces with rms values higher than 20 nm above which the cell adhesion, proliferation and morphology was significantly affected. Thus, in the case of

primary human fibroblasts, culture on the roughest surfaces led to the reduction of adhered cell number and their proliferation rate, as well as to significant shrinkage of cell cytoplasm and nucleus area, indicating a fatal effect of rough surfaces on these cells. On the other hand, despite the fact that the number and proliferation of immortalized mouse 3T3 fibroblasts was affected on all rough surfaces, the strongest effect was again observed when cells were cultured on surfaces with rms values higher than 20 nm, where in addition a strong effect on cell morphology was observed. Given the different stiffness and size of two cell types, the similarity of roughness thresholds may seem puzzling. In an attempt to explain it, two different theoretical approaches [35-37] have been reconciled emphasizing the double role that elasticity and size may have in cell viability on rough surfaces: on one side, they enhance adhesion areas on surface protrusions increasing the capturing strength while on the other side, they induce more stretching of the suspended cell membrane deteriorating cell functions and viability. These two effects can counteract and cause similar roughness thresholds in cell series with different stiffness and size. The understanding of the response of different cell types to nanotopography and the control of cell adhesion and morphology based on the effect of substrate micro-nanotopography could provide essential information for the design of novel materials [18, 20] for incorporation in "smart" microarrays, microfluidics, and lab on chip devices for in vitro and in vivo applications.

5. References

[1] Bettinger C J, Langer R and Borenstein J T 2009 Angew. Chem. Int. Ed. Engl. **48** 5406-15

[2] Gasiorowski J Z, Murphy C J and Nealey P F 2013 Annu. Rev. Biomed. Eng. **15** 155-76

[3] Kim H N, Jiao A, Hwang N S, Kim M S, Kang do H, Kim D H and Suh K Y 2013 Adv. Drug. Deliv. Rev. **65** 536-58

[4] Joanne P, et al. 2016 Biomaterials **80** 157-168

[5] Kearns V R, Mc Murray R J and Dalby M J 2011 Biomaterial surface topography to control cellular response: technologies, cell behavior and biomedical applications Surface modification of biomaterials Methods, analysis and applications (Oxford: Woodhead Publishing Limited) pp 169-201

[6] Goto M, Tsukahara T, Sato K and Kitamori T 2008 Anal. Bioanal. Chem. **390** 817-23

[7] Trantidou T, Terracciano C M, Kontziampasis D, Humphrey E J and Prodromakis T 2015 Sci. Report **5** 11067

[8] Singh A V, Patil R, Thombre D K and Gade W N 2013 J. Biomed. Mater. Res. Part A **101** 3019-3032

[9] Anselme K, Davidson P, Popa A M, Giazzon M, Liley M and Ploux L Acta Biomater. 2010 **6** 3824-46

[10] Idota N, Tsukahara T, Sato K, Okano T and Kitamori T 2009 Biomaterials **30** 2095-101

[11] Wood M A 2007 J. R. Soc. Interface **4** 1-17

[12] O'Connell C D, Higgins M J, Moulton S E and Wallace G G 2015 J. Mater. Chem. C **3** 6431-6444

[13] Ruiz S A and Chen C S Soft Matter 2007 **3** 168-177

[14] Dalby M J, Pasqui D and Affrossman S IEEE Proc. Nanobiotechnol. **151** 53-61

[15] Jayasinghe S N 2013 Analyst **138** 2215-23

[16] Spijker H T, Bos R, Busscher H J, van Kooten T G and van Oeveren W 2002 Biomaterials **23** 757-766

[17] Tsougeni K, Vourdas N, Tserepi A and Gogolides E 2009 Langmuir **25** 11748-11759

[18] Tsougeni K, Bourkoula A, Petrou P, Tserepi A, Kakabakos S E and Gogolides E 2014 Microelectron. Eng. **124** 47-52

[19] Gogolides E, Constantoudis V, Kokkoris G, Kontziampasis D, Tsougeni K, Boulousis G, Vlachopoulou M and Tserepi A 2011 J. Phys. D: Applied Physics **44**, 174021.

[20] Gogolides E, Ellinas K and Tserepi A 2015 Microelectron. Eng. **132** 135-155

[21] Vourdas N, Kontziampasis D, Kokkoris G, Constantoudis V, Goodyear A, Tserepi A, Cooke M and Gogolides E 2010 Nanotechnology **21** 085302.

[22] Kontziampasis D, Constantoudis V and Gogolides E 2012 Plasma Proc. Polymer **9** 866-872.

[23] Tserepi A, Gogolides E, Bourkoula A, Kanioura A, Kokkoris G, Petrou P S and Kakabakos S E Plasma Chem. Plasma Proc. 2016 **36** 107-120

[24] Loesberg W A, Riet J, van Delft F C M J M, Schön P, Figdor C G, Speller S, van Loon J J W A, Walboomers X F and Jansen J A 2007 Biomaterials **28** 3944-51

[25] Dalby M J, Riehle M O, Johnstone H, Affrossman S and Curtis A S 2002 Biomaterials **14** 2945-54

[26] Dalby M J, Riehle M O, Johnstone H J, Affrossman S and Curtis A S 2002 Tissue Eng. **8** 1099-108

[27] Kunzler T P, Huwiler C, Drobek T, Vörös J and Spencer N D 2007 Biomaterials 28 5000-6

[28] Li B and Logan B E 2004 Colloid Surf. B Biointerfaces **36** 81-90

[29] Webster T-J and Ejiofor J U 2004 Biomaterials **25** 4731-9

[30] de Oliveira P T, Zalzal S F, Beloti M M, Rosa A L and Nanci A 2007 J. Biomed. Mater. Res. A **80** 554-64

[31] Fan Y W, Cui F Z, Hou S P, Xu Q Y, Chen L N and Lee I S 2002 J. Neurosci. Methods **120** 17-23

[32] Gentile F, Tirinato L, Battista E, Causa F, Liberale C and Decuzzi P 2010 Biomaterials **31** 7205-7212

[33] Davidson P M, Bigerelle M, Reiter G and Anselme K 2015 Biointerphases **10** 031004

[34] Kontziampasis D, Bourkoula A, Petrou P, Tserepi A, Kakabakos S and Gogolides E 2013 Proc. SPIE **8765** 87650B

[35] Decuzzi P and Ferrari M 2006 Biomaterials **27** 5307-5314

[36] Ivanova E P, et al. 2012 Small **8** 2489-2494

[37] Pogodin S, et al. 2013 Biophys. J. **104** 835-840

[38] Efremov Y M, Lomakina M E, Bagrov D V, Makhnovskiy P I, Alexandrova A Y, Kirpichnikov M P and Shaitan K V 2014 Biochim. Biophys. Acta **1843** 1013-1019

[39] Constantoudis V, Patsis G P, Leunissen L H A and Gogolides E 2004 J. Vac. Sci. Technol. B **22**, 1974 -1981

[40] Xue F, Liu J, Guo L, Zhang L, Li Q 2015 J. Theor. Biol. **385** 1-7

[41] Tsougeni K, Vourdas N, Tserepi A and Gogolides E, 2015 ACS Appl. Mater. Interfaces **7** 14670–14681

[42] Huth F, Govyadinov A, Amarie S, Nuansing W, Keilmann F and Hillenbrand R 2012 Nano Lett. **12** 3973–3978

[43] Emmons E D, Kraus R G, Duvvuri S S, Thompson J S and Covington A M 2007 J. Polym. Sci. Part B: Polym. Phys. **45** 358–367